Neutron capture cross section of ^{53}Mn from irradiation with cold and reactor neutrons

J. Ulrich,[1] M. Ayranov,[1] A. Kaestner,[1] D. Schumann,[1] P. Sprung,[1] A. Türler,[2] L. Viererbl,[3] M. Vinš,[3] H. Assmann-Vratislavská,[3] and R. Dressler[1,*]

[1]*Paul Scherrer Institute, CH-5232 Villigen, Switzerland*

[2]*Departement of Chemistry and Biochemistry, Universität Bern, CH-3012 Bern, Switzerland*

[3]*Research Centre Řež, 250 68 Husinec-Řež, Czech Republic*

(Received 26 February 2020; accepted 23 April 2020; published 12 August 2020)

The neutron capture cross section of ^{53}Mn was measured with cold and reactor neutrons by the activation method, relative to the well-known cross section of ^{59}Co. Three targets containing a total of $\approx 10^{18}$ atoms ^{53}Mn in the form of chloride salt were prepared using a stock solution obtained from activated accelerator waste in the course of the ERAWAST initiative at Paul Scherrer Institute, Switzerland (PSI). Natural cobalt salt was added to the sample material as an internal neutron flux monitor. The total numbers of ^{53}Mn and ^{59}Co atoms in the target were deduced via mass spectrometric measurements at PSI. Cold-neutron activation was carried out at the ICON beamline at PSI. Reactor activation was performed at the LVR-15 research reactor of Research Centre Řež in a well-moderated neutron field of an outer reactor channel. The thermal-neutron capture cross section and the resonance integral were determined by the cadmium ratio method. The induced activities of ^{54}Mn and ^{60}Co were quantified by high-resolution γ-ray spectrometry. The obtained thermal-neutron capture cross section of 76.5 ± 1.4 b agrees well with previously reported results. The uncertainty of this value could be reduced by almost an order of magnitude with respect to older measurements and is on a level comparable to stable nuclides. The resonance integral of 43.1 ± 1.2 b was obtained for the real reactor spectrum with epithermal-spectrum shape factor $\alpha = 0.025$.

DOI: 10.1103/PhysRevC.102.024613

I. INTRODUCTION

^{53}Mn ($t_{1/2} \approx 3.7$ Ma) is expected to be one of the major short-lived radionuclides produced during core-collapse supernovae explosions [1,2]. It can undergo further nuclear reactions due to its long half-life, which may influence the isotopic abundances of neighboring stable isotopes. Additionally, it can serve as a sensitive chronometer to date processes in the early solar system [3] and to determine the exposure time of terrestrial material to high energetic cosmic radiation [4].

The thermal-neutron capture cross-section measurements reported in [5–8] are the only ones performed to determine any neutron capture cross section of ^{53}Mn so far. Millard Jr. [5] and Honda *et al.* [6,7] irradiated samples containing ^{53}Mn extracted from meteoritic material in a research reactor and deduced the cross section from the ^{54}Mn production. Wölfle *et al.* [8] obtained the cross section measuring the decrease of the ^{54}Mn production rate due to ^{53}Mn burn-up during a 587 day long reactor activation. A thermal-neutron capture cross-section value of 70 ± 10 b is given in the current edition of the Atlas of Neutron Resonances by Mughabghab [9], based on these measurements. This value is nowadays used as a reference, e.g., for anchoring the ^{53}Mn(n,γ) cross sections predicted on the base of nuclear models available in the TENDL evaluated nuclear data library [10–14].

Neutron activation analysis (NAA) has been a very sensitive method to quantify the total content of ^{53}Mn, used since the beginning of the measurements of this isotope in meteoritic or geological samples. Englert *et al.* [15] demonstrated the high sensitivity of NAA, which is capable of reaching detection limits of 10^{-14} g ^{53}Mn per g iron matrix. At present, accelerator mass spectrometry (AMS) is capable of realizing detection limits of 10^{-16} g/g [4]. However, samples with such extremely low ^{53}Mn concentrations are not common. Typically the ^{53}Mn concentration ranges from 10^{-14} g/g [4] as a lower bound for terrestrial samples to 10^{-9} g/g [15] as a upper bound for meteorite samples. Therefore, NAA remains a very convenient technique for ^{53}Mn quantification in both types of samples, as recently discussed by Yants *et al.* [16]. If the ^{53}Mn to ^{55}Mn ratio is sufficiently high, NAA will have a practical advantage over AMS due to the overall lower cost, less complex sample preparation and higher sample throughput. Since a basic requirement for NAA is the precise value of the neutron capture cross section, a reduction of its uncertainty is directly transformed into an improvement in the accuracy of the NAA results.

In the framework of the ERAWAST project [17], various rare and exotic radionuclides for research and application have been extracted from a large variety of accelerator originated sources (components of the accelerator, muon production targets, beam dumps, irradiated test samples, as well as specially designed filter devices installed into the cooling circuits). The source of the ^{53}Mn material used in this experiment was the copper beam dump of the former "Bio-Medical-Area" at PSI, which was irradiated with a 590 MeV proton beam delivered by the PSI ring cyclotron with an integrated dose of about

*rugard.dressler@psi.ch

0.16 Ah. The measured concentration of ^{53}Mn close to the beam axis was about 10^{18} atoms per g copper [18]. About 500 g of highly radioactive copper chips were collected before the final disposal of the remaining parts of the beam dump and served as source of ^{53}Mn and other exotic nuclides. As of today, several 10^{18} atoms ^{53}Mn were extracted from about 5 g of the Cu beam dump material, purified and made available for various experiments.

The principal limiting factor of the previous experiments was the small available amount of ^{53}Mn. The experiment with the largest amount of ^{53}Mn conducted so far is the cross-section measurement of Wölfle *et al.* [8]. A manganese fraction of 2 g was extracted from total 20 g material of the Duchesne nickel-iron meteorite. This fraction contained about 1.8×10^{13} atoms of ^{53}Mn. Apart from the measurement by Wölfle [8], the other cross-section values also depend on the half-life of ^{53}Mn (not better known today than 10%), since the number of target atoms was deduced from ^{53}Mn activity measurements. This approach introduces an additional possible systematic uncertainty as the detectors were calibrated using ^{54}Mn, which emits relaxation radiation with identical energies as ^{53}Mn. However, in the case of ^{54}Mn the electron-capture decay is allowed whereas it is second forbidden non-unique for ^{53}Mn according to the systematics of β-decay. This can cause significant differences in electron-capture probabilities from the individual electron shells and, thus, different probabilities of the characteristic x-ray emission for both radionuclides. The amount of material available for our experiment ($\approx 10^{18}$ atoms ^{53}Mn) is about a factor of 10 000 larger than samples of ^{53}Mn used in the previous studies which were extracted from meteoritic material. This is sufficient to obtain ^{54}Mn activities in the order of 100–1000 Bq even after short irradiation times with currently available cold- or thermal-neutron fluxes. In addition, the direct measurement of ^{53}Mn atom concentrations via inductively coupled plasma mass spectrometry (ICP-MS) is possible today.

All uncertainties are calculated according to the Guide to the expression of uncertainty in measurement [19] and are quoted with a coverage factor $k = 1$, i.e., confidence level of about 68%, if not stated otherwise.

II. MATERIALS AND METHODS

A. Sample production

The purified ^{53}Mn fraction [20] in the form of an acidic chloride solution was evaporated to dryness and redissolved in approx. 0.5 mL 1 M HCl. This solution was spiked with 20 μL natural cobalt chloride solution ($\approx$100 mg/mL $CoCl_2.6H_2O$ in Milli-Q water) with the purpose to act as internal neutron flux monitor during the activation experiments, utilizing the reaction ^{59}Co(n, γ) ^{60}Co. Three individual samples were prepared by dropping this solution on a glass wool filter disk with a diameter of 0.6 cm, fixed on transparent pressure-sensitive adhesive tape (PSA tape). Six droplets of the solution were successively deposited on each filter disk. After each droplet, the liquid was evaporated to dryness by putting the samples on a hot ($\approx$120 °C) heating plate, leaving a solid salt residue inside and on top of the filter. The exact amounts of the stock solution deposited on each target were traced gravimetrically. The final drying of the samples was performed in a drying cabinet (110 °C, 60 min).

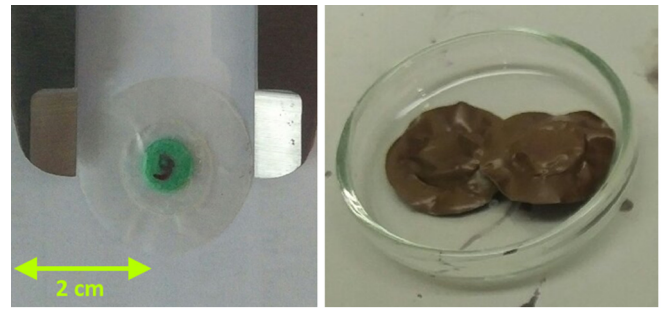

(a) (b)

FIG. 1. One of the prepared ^{53}Mn samples before the activation experiments (left) and together with the dummy target after the 3 h reactor activation (right).

Subsequently, the samples were covered by a second strip of PSA tape, forming a sandwich with the salt-loaded filter between two layers of PSA tape, positioned with their adhesive-covered sides towards each other. A disk of 1.0 cm diameter was punched out of this assembly, leaving a 0.2 cm wide rim around the centrally positioned filter. To prevent moisture uptake by the strongly hygroscopic salt, the samples were additionally fixed between a second set of two discs of PSA tape of 2.6 cm diameter. The left panel of Fig. 1(a) shows one of the finished samples. A retained sample of the stock solution was kept aside for the later analysis of the isotopic composition and the total ^{53}Mn and ^{59}Co content. The exact amount was traced gravimetrically.

B. Sample characterization

^{55}Mn and ^{59}Co contents in the stock solution were determined by multicollector ICP-MS (MC-ICP-MS) using gravimetric standard addition with Fe as an internal standard [21,22] and reverse isotope dilution [23]. The absolute number of ^{53}Mn atoms in the stock solutions used for the sample preparation was obtained from the measured ^{53}Mn/^{55}Mn isotopic ratio of a Mn-standard-free analyte. The ^{53}Mn signal was corrected for isobaric interference from ^{53}Cr by monitoring ^{52}Cr and using the measured value ^{53}Cr / ^{52}Cr $= 0.167314 \pm 0.000014$ of the isotopic ratio. This value is strongly shifted towards ^{53}Cr in comparison with the natural abundance of ^{53}Cr / ^{52}Cr $= 0.113386 \pm 0.000073$ [24] as a result of the long-term irradiation of the copper material. To obtain the ^{53}Cr/^{52}Cr isotopic ratio, the Cr in the stock solution was chemically separated from Mn utilizing the method described in [25], followed by measuring the isotopic ratio of the Mn-free fraction using the same ICP-MS measurement scheme as described above.

All mass spectrometric measurements were conducted using a Plasma 3 MC-ICP-MS designed and manufactured by Nu Instruments at a resolving power above 8000 [26]. All solutions were introduced via a self-aspiring PFA-ST MicroFlow nebulizer at approx. 50 μL/min uptake rate and an Apex HF desolvating nebulizer (both from Elemental

TABLE I. Number of atoms N of ^{53}Mn and ^{59}Co in the three samples used for activation experiments, based on MC-ICP-MS analysis of the stock solution and the amounts m of the stock used for preparation of each sample.

		Sample 1	Sample 2	Sample 3
m (mg)		120.39 ± 0.06	132.40 ± 0.06	115.83 ± 0.06
N (10^{17})	^{53}Mn	3.180 ± 0.014	3.497 ± 0.015	3.059 ± 0.013
	^{59}Co	7.887 ± 0.048	8.673 ± 0.053	7.588 ± 0.046

Scientific). All ion beams from mass 52 (Cr) up to 59 (Co) were collected simultaneously in Faraday cups connected to amplifiers with 10^{11} Ω resistors in their feedback loop. The instrumental signal on each cup was background corrected by subtracting the signal obtained during 120 s of measurement prior to each analyte supplying the identical 0.28 M HNO_3 solution that was used in the preparation of all standard and sample analytes.

The isotopic ratio of each sample and standard measurement is represented by the average of 100 individual 10-s-long integrations. Instrumental mass discrimination was characterized and corrected for using an exponential law [27]. The nuclide masses from the atomic mass evaluation [28] were used. Instrumental mass-discrimination corrections for samples were done normalizing either internally to ^{57}Fe / ^{56}Fe = 0.023096 ± 0.000036 [29] or externally, intermittently analyzing mixed natural Fe-Cr standard solutions at equivalent signal intensities and using the mass-discrimination information obtained by normalizing their ^{57}Fe / ^{56}Fe or ^{53}Cr / ^{52}Cr isotopic ratios to those taken from the literature. The external mass-discrimination scheme allowed including additional data.

Final uncertainties are derived by Monte Carlo uncertainty propagation that includes: (i) the certified concentration uncertainties of the utilized TraceCert ^{55}Mn and ^{59}Co reference solutions, (ii) weighing uncertainties obtained from repeatedly weighing each dilution and additional steps during preparation of the stock-standard-mixtures analyzed for standard addition and isotope dilution, (iii) the uncertainties of repeated mass spectrometric analyses of each stock-standard-mixtures, and (iv) the overall scatter in concentration results from combining the individual results for each of the four stock-standard-mixtures with that obtained for the Mn-standard-free analyte of the same stock. Step (iv) is considered more robust than regressing the five data points for Mn-standard-free analyte and the stock-standard-mixtures because it reflects that the actually measured Mn-standard-free composition defines the y intercept of standard-addition regressions and, thus, prevents possible bias in the value induced by scatter in the data for the stock-standard-mixtures.

The concentrations of ^{53}Mn and ^{59}Co in the stock solution were determined to be $(1.403 \pm 0.006) \times 10^{17}$ g^{-1} and $(3.48 \pm 0.02) \times 10^{17}$ g^{-1}, respectively. The amounts of ^{53}Mn and ^{59}Co atoms present in each sample are given in Table I.

C. Cold-neutron activation

The activation experiment with cold neutrons was carried out at the ICON beamline [30] of the PSI spallation neutron source SINQ with a mean neutron energy of 8.53 meV. Fig. 2 shows the neutron spectrum determined at the beamport by time-of-flight measurements [30,31]. The ICON beamline is a user facility with primary focus on cold-neutron imaging. The activation of the samples was performed in parasitic mode, i.e., concurrently to other user experiments running at the beamline. The impact on the other user experiments was minimal, with only a slight vignetting for experiments using the largest neutron field. An aluminum sample holder was designed and manufactured, which could be mounted behind the beam shutter and let most of the beam pass unobstructed through the central rectangular opening (see Fig. 3). In the corners of this opening, up to four samples with a maximum size of approximately 1 × 1 cm^2 can be placed. In our experiments, three positions were occupied with the ^{53}Mn containing samples and one by a Cividec B6C neutron-sensitive diamond detector used for online flux monitoring. The count-rate readout and the data recording was realized via LabVIEW. The neutron flux at the corner positions varies by two orders of magnitude in dependence of the collimating aperture diameter used for the particular imaging experiment (typically 2.0 cm, 4.0 cm, and 8.0 cm opening diameter). Therefore, the activation was scheduled into a time slot, in which a frequent usage of the largest (diameter of 8.0 cm) aperture was planned, thus providing

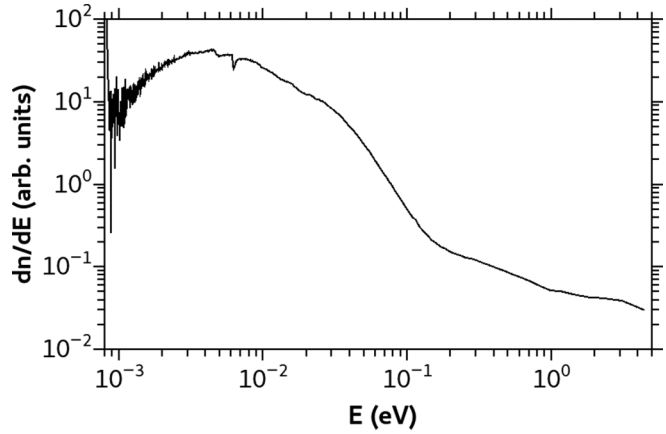

FIG. 2. Neutron spectrum at the ICON beamline [30,31]; the average neutron energy is 8.53 meV.

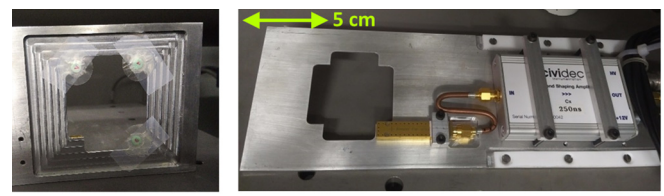

FIG. 3. Front side (from direction of the beam) of the setup for activation at ICON with mounted samples on three positions (left). Rear side with attached neutron detector and preamplifier. The opening enables passing of the majority of the beam. The samples are mounted at the corners of the opening.

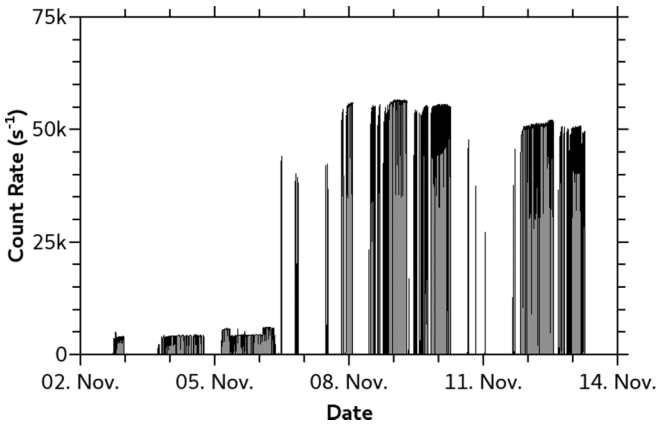

FIG. 4. Intensity of the neutron beam at the sample positions during the cold-neutron activation experiment as recorded by the neutron-sensitive detector. Count rates of about 50 kCPS correspond to the large ($\phi = 8.0$ cm), 5 kCPS to the middle ($\phi = 4.0$ cm) aperture.

the highest neutron flux at the sample positions. The samples were irradiated for 12 d in total, Fig. 4 presents the measured counts per second (CPS) of the neutron detector during the time period of the experiment. This was used as a measure of the momentary neutron beam intensity at the sample positions during the irradiation.

D. Reactor neutron activation

The second activation of the samples was performed in the LVR-15 reactor at Research Centre Řež about five months after the activation with cold neutrons. LVR-15 is a light-water research reactor with a maximum thermal power of 10 MW and maximum thermal-neutron flux of 10^{14} cm^{-2}s^{-1}. Figure 5 shows the core layout during the time where the ^{53}Mn experiments were performed. The samples were irradiated inside of an aluminum capsule at the position "DONA 6" (DN-6, see Fig. 5) in the outer region of the reactor core to assure a well-moderated neutron spectrum [32].

For neutron fluence evaluation, activation detectors of Fe, Ni, Co (1% alloy with Al), and Zn with a diameter of 4.0 mm and a thickness of 0.1 mm were used. Relevant dosimetry reactions are ^{54}Fe$(n, p)^{54}$Mn, ^{58}Fe$(n, \gamma)^{59}$Fe, ^{58}Ni$(n, p)^{58}$Co, ^{59}Co$(n, \gamma)^{60}$Co, and ^{64}Zn$(n, \gamma)^{65}$Zn. The induced activities were later measured with HPGe detector and the reaction rates were deduced. The theoretical neutron spectrum was calculated with the MCNP code [33] and used as input spectrum for spectral adjustments with the STAYSL PNNL software suite [34].

As the samples were cooled directly by the primary reactor coolant at 50 °C – 60 °C, streaming through the inner volume of the capsule, they were placed in two layers of welded plastic bags to prevent contamination. In addition, three "dummy" samples were prepared in analogous way like the ^{53}Mn samples, but using a mixed solution of natural iron, cobalt and manganese chlorides in similar concentrations like in the ^{53}Mn stock solution. One of these dummy samples was placed in the bag with the real sample during each irradiation.

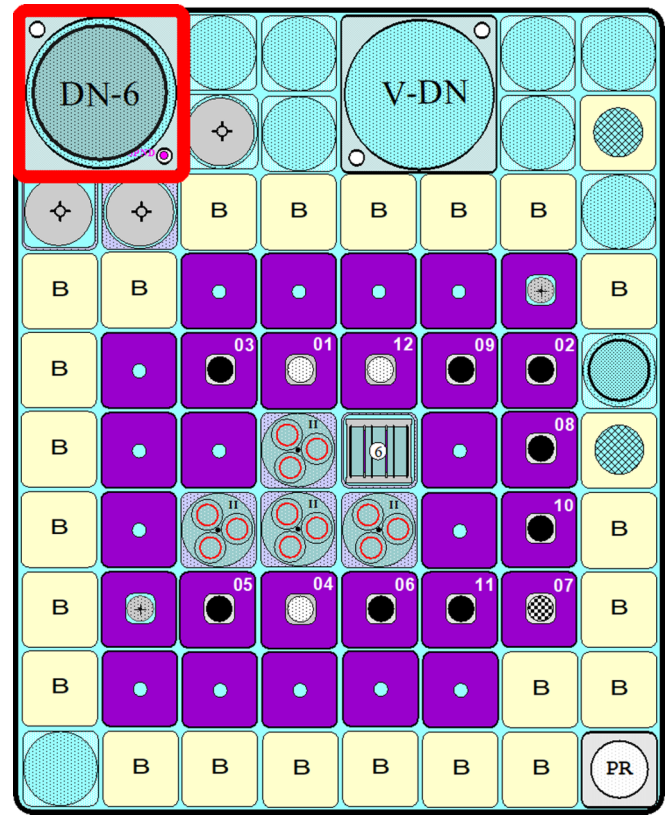

FIG. 5. Core layout of LVR-15 in the reactor cycle at the time of ^{53}Mn activation. Color coding: fuel assemblies – purple, beryllium reflectors – yellow, water and irradiation channels – cyan. The irradiation position DONA 6 is highlighted in red.

The purpose of the dummy samples was to investigate the possibility of a significant ^{54}Mn production by fast-neutron reactions on the unseparated impurities in the ^{53}Mn sample. No ^{54}Mn activity could be measured in these dummies after the irradiation.

Samples 1 and 2 were irradiated bare, sample 3 was irradiated inside of a cylindrical cadmium case with wall thickness of 0.5 mm and outer height and diameter of 6.1 mm and 23.2 mm, respectively. Metal foil flux monitors were put next to samples in the capsule in order to measure the absolute neutron fluence and spectrum. Samples 1 and 2 were irradiated for 25 min, sample 3 for 180 min. The intense γ-ray radiation in the reactor core caused a visible coloring of the transparent PSA tape, especially for sample 3 due to the longer irradiation period [see Fig. 1(b)].

E. Activation measurements

The produced amounts of the activation products ^{54}Mn and ^{60}Co were quantified by high-resolution γ-ray spectrometry. The activity of each sample was measured after preparation, after the cold-neutron activation and after the reactor activation, respectively. The activities produced in the particular experiment were obtained as a difference between sample measurements before and after the corresponding irradiation.

TABLE II. Half-lives $t_{1/2}$, γ-ray energies E and emission probabilities I_γ of ^{54}Mn and ^{60}Co as well as corresponding FEP efficiencies ε, determined for the geometry of the measurements. Nuclear data from [35] were adopted.

	$t_{1/2}$ (d)	E (keV)	I_γ (%)	ε (%)
^{54}Mn	312.19 ± 0.03	834.848 ± 0.003	99.9752 ± 0.0005	0.2106 ± 0.0021
^{60}Co	1925.2 ± 0.3	1173.228 ± 0.003	99.85 ± 0.03	0.1503 ± 0.0017
		1332.492 ± 0.004	99.9826 ± 0.0006	0.1310 ± 0.0015

The samples were measured with a Broad Energy Germanium Detector (Canberra BEGe 2825, 18% relative efficiency) in distance of 9 cm from the detector endcap using a dedicated sample holder. The full-energy-peak (FEP) efficiency calibration was performed using a calibration source with kBq amounts of ^{54}Mn and ^{60}Co, fabricated in analogous manner as the real samples (see Sec. II A) to account in the best possible way for the real sample geometry, activity distribution in the filter disk and γ-ray self-absorption within the sample. A radionuclide solution containing both ^{54}Mn and ^{60}Co and characterized in terms of specific activity of both radionuclides was used for preparing the calibration source. The precise activity of the calibration source was then obtained from the mass of the solution spent for preparation of the source. Table II summarizes the determined FEP efficiencies ε. The half-lives $t_{1/2}$, the γ-ray energies E, and the emission probabilities I_γ taken from the compilation [35] were used for all ^{54}Mn and ^{60}Co activity measurements. Table III gives an overview of the results of the activity measurements.

III. DATA EVALUATION

A. Cold-neutron cross section

The actual quantity measured in the experiment is not the cross section σ_{Mn} of the neutron capture reaction $^{53}\mathrm{Mn}(n,\gamma)^{54}\mathrm{Mn}$ itself, but the cross-section ratio r_σ, i.e., the relative magnitude of σ_{Mn} compared to σ_{Co}, the cross section of the reaction $^{59}\mathrm{Co}(n,\gamma)^{60}\mathrm{Co}$. ^{59}Co serves as internal flux monitor during the measurements, assuming a strict $1/v$ dependence of the cross section

$$r_\sigma = \frac{\sigma_{\mathrm{Mn}}}{\sigma_{\mathrm{Co}}} = \frac{Y_{\mathrm{Mn}}}{Y_{\mathrm{Co}}} \tag{1}$$

with

$$Y = \frac{\Delta A_1 t_{1/2}}{N k_{\mathrm{dec}} G}, \tag{2}$$

where N denotes the number of atoms in the target (see Table I), $t_{1/2}$ is the half-life of the corresponding activation product (^{54}Mn or ^{60}Co), G is the neutron self-shielding factor, and k_{dec} is a factor correcting for the decay of the activation products during the irradiation period. The factor k_{dec} was calculated for both radionuclides using the irradiation history (see Fig. 4) as follows:

$$k_{\mathrm{dec}} = \frac{\sum_i Z_i \exp\left(-\frac{\ln(2)\Delta t}{t_{1/2}}\right)}{\sum_i Z_i}. \tag{3}$$

The terms in the numerator and denominator sum over individual entries i in the log file of the neutron flux measurement. Δt_i gives the time difference between the recorded timestamp of the entry and the reference time of the activity values, Z_i is the count-rate of the neutron detector. As the irradiation period was rather short, compared to the half-lives of both activation products, the values of k_{dec} are very close to unity (99.17% and 99.86% for ^{54}Mn and ^{60}Co, respectively). The uncertainty of k_{dec} is well below 0.01% in both cases and was neglected in further calculations.

The neutron self-shielding factor G was assumed to be identical for both ^{53}Mn and ^{59}Co, as the samples were prepared from an aqueous solution containing both nuclides and a homogenous mixture of both isotopes is expected to be kept within the solid salt precipitated after evaporation of the solution. Thus, these terms cancel out in Eq. (1). Table IV reports the values of r_σ and the deduced capture cross sections $\sigma_{0,\mathrm{Mn}}$ for thermal neutrons with velocity $v = 2200$ m/s (corresponding to a kinetic neutron energy of 25.3 meV),

TABLE III. Pre- and post-irradiation activities of the samples as determined by γ-ray spectrometry and the resulting induced activities ΔA. Index "1" denotes the first, cold-neutron activation, index "2" the reactor activation. The reference times of the activities are 14.11.2017 00:00:00 for cold-neutron activation and 29.03.2018 13:00:00 for reactor activation and correspond roughly to the end of the particular irradiation. The values of $A_{2,\mathrm{pre}}$ were obtained by recalculation of $A_{1,\mathrm{post}}$ to the new reference date.

	Sample 1		Sample 2		Sample 3	
	^{54}Mn	^{60}Co	^{54}Mn	^{60}Co	^{54}Mn	^{60}Co
$A_{1,\mathrm{pre}}$ (Bq)	<0.5	4.26 ± 0.30	<0.5	4.45 ± 0.29	<0.5	4.35 ± 0.28
$A_{1,\mathrm{post}}$ (Bq)	144.1 ± 1.5	33.19 ± 0.46	200.0 ± 2.1	44.26 ± 0.58	185.2 ± 2.0	41.21 ± 0.55
ΔA_1 (Bq)	144.1 ± 1.5	28.94 ± 0.52	200.0 ± 2.1	39.81 ± 0.61	185.2 ± 2.0	36.85 ± 0.58
$A_{2,\mathrm{pre}}$ (Bq)	106.7 ± 1.1	31.61 ± 0.44	148.1 ± 1.5	42.15 ± 0.55	137.1 ± 1.4	39.25 ± 0.52
$A_{2,\mathrm{post}}$ (Bq)	8560 ± 85	1707 ± 20	9639 ± 96	1920 ± 22	556.5 ± 5.7	340.8 ± 3.9
ΔA_2 (Bq)	8453 ± 84	1676 ± 19	9491 ± 95	1878 ± 21	419.5 ± 4.4	301.6 ± 3.5

TABLE IV. Cross-section ratios r_σ measured by cold-neutron activation and neutron capture cross sections $\sigma_{0,\mathrm{Mn}}$ of ^{53}Mn deduced on the base of these ratios. Additionally, the nuclear data and decay correction factors k_{dec} required for calculation according to Eq. (2) are listed.

	Sample 1	Sample 2	Sample 3
$k_{\mathrm{dec,Co}}$		99.86%	
$k_{\mathrm{dec,Mn}}$		99.17%	
r_σ	2.017 ± 0.045	2.036 ± 0.041	2.035 ± 0.041
$\sigma_{0,\mathrm{Mn}}$ (b)	75.0 ± 1.7	75.7 ± 1.5	75.7 ± 1.5

calculated individually for each sample using the adopted value of $\sigma_{0,\mathrm{Co}} = 37.18 \pm 0.06$ b [9].

B. Reactor spectrum

The measured fluxes of thermal (<0.5 eV), epithermal (0.5 eV–100 keV) and fast (>100 keV) neutrons together with the irradiation times t_{irr} for all three samples are presented in Table V and the calculated neutron spectra are given in Fig. 6. The flux monitor foils were mounted externally on the cadmium shielding during activation of sample 3 (see Sec. II D). Thus, the measured thermal-neutron flux is not representative for the real neutron flux applied to the sample located inside of the cadmium shielding. As can be seen on Fig. 6, the thermal flux outside of the cadmium case is only about 50% lower due to the local perturbation of the thermal-neutron field in the vicinity of the case. The calculated fluences and spectral shapes for samples 1 and 2 are almost identical. The epithermal and fast regions of the neutron spectrum for sample 3 are not significantly affected by the presence of cadmium and their shapes matches those of samples 1 and 2.

For better normalization of the activation rates in the further analysis, the factor k_ϕ was introduced, accounting for the variations of the total neutron flux magnitude between individual activations. k_ϕ was defined as the ratio of the particular fast-neutron flux to the fast-neutron flux during the activation of sample 1. The fast-neutron flux was chosen as a representative measure of the total neutron flux magnitude as it is at least affected by the presence of the cadmium shielding.

The shape of the neutron spectrum in epithermal range is described by a $1/E^{1+\alpha}$ behavior. The epithermal-spectrum shape factor $\alpha = 0.025 \pm 0.003$, quantifying the deviation

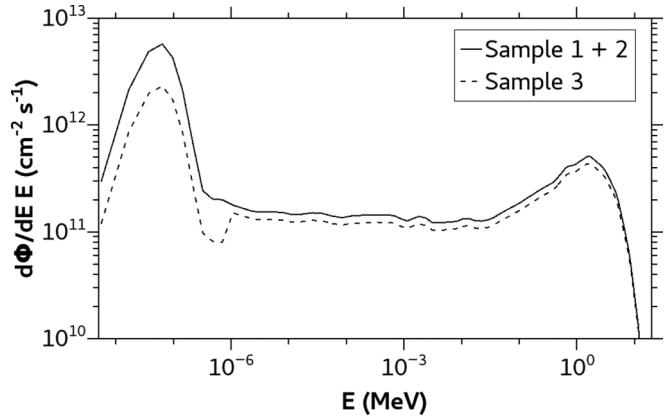

FIG. 6. Calculated neutron flux spectra during reactor activations of samples 1–3. The magnitude and shape differences between sample 1 and 2 spectra are not distinguishable in the plot. Hence, the filled curve is representative for both samples 1 and 2.

of the epithermal part of the spectrum from an ideal $1/E$ shape, was obtained by fitting the calculated neutron spectrum between 2 eV and 30 keV. The energy dependence of α was neglected.

C. Thermal-neutron cross section and resonance integral calculation

The activation rates R per atom ^{53}Mn and ^{59}Co during the reactor activation were calculated using the relation

$$R = \frac{\Delta A_2 t_{1/2}}{N t_{\mathrm{irr}} k_\phi \ln(2)}. \tag{4}$$

The deduced activation rates R and the cadmium ratios C, i.e., the ratios between the activation rate with and without cadmium shield are given in Table VI. In case of a well-moderated neutron spectrum, the activation rate R in the neutron field with thermal- and epithermal-components can be formulated as a sum of thermal- and epithermal-activation rates R_{th} and R_{epi} using the Høgdal convention [36,37]

$$R = R_{\mathrm{th}} + R_{\mathrm{epi}} = \phi_{\mathrm{th}} g_w \sigma_0 G_{\mathrm{th}} + \phi_{\mathrm{epi}} I_0(\alpha) G_{\mathrm{epi}} \tag{5}$$

with the thermal- and epithermal-neutron fluxes ϕ_{th} and the ϕ_{epi}, corresponding self-shielding factors G_{th} and G_{epi}, the Westcott factor g_w, the capture cross sections σ_0

TABLE V. Irradiation periods t_{irr} and energy-dependent neutron fluxes calculated using co-activated neutron flux monitor foils.

	Sample 1	Sample 2	Sample 3
Thermal (cm^{-2} s^{-1}) (<0.5 eV)	$(1.122 \pm 0.029) \times 10^{13}$	$(1.107 \pm 0.029) \times 10^{13}$	$(4.53 \pm 0.12) \times 10^{12}$
Epithermal (cm^{-2} s^{-1}) (0.5 eV–100 keV)	$(1.778 \pm 0.066) \times 10^{12}$	$(1.753 \pm 0.065) \times 10^{12}$	$(1.512 \pm 0.061) \times 10^{12}$
Fast (cm^{-2} s^{-1}) (100 keV–2 MeV)	$(1.402 \pm 0.042) \times 10^{12}$	$(1.382 \pm 0.042) \times 10^{12}$	$(1.2011 \pm 0.038) \times 10^{12}$
t_{irr} (s)	1500	1500	10800
k_ϕ (%)	100.0	98.6	85.7

TABLE VI. Measured activation rates R and cadmium ratios C as well as the resulting cross sections $\sigma_{0,\mathrm{Mn}}$ at $v = 2200$ m/s and the resonance integrals $I_{0,\mathrm{Mn}}(\alpha)$ of ^{53}Mn and the ratio of these quantities $Q_{0,\mathrm{Mn}}(\alpha)$. Whereas the values of R_{Mn} and R_{Co} originate from the activation of sample 1 or sample 2 as indicated by the corresponding column titles, $R_{\mathrm{epi,Mn}}$ and $R_{\mathrm{epi,Co}}$ were deduced from the activation of sample 3 inside of the Cd case and are the same for samples 1 and 2. This approach is justified as all activation rates were properly normalized per target atom and flux intensity [see Eq. (4)].

	Sample 1	Sample 2
R_{Mn} (s^{-1})	$(6.897 \pm 0.075) \times 10^{-10}$	$(7.143 \pm 0.078) \times 10^{-10}$
R_{Co} (s^{-1})	$(3.399 \pm 0.044) \times 10^{-10}$	$(3.514 \pm 0.045) \times 10^{-10}$
$R_{\mathrm{epi,Mn}}$ (s^{-1})	$(5.766 \pm 0.065) \times 10^{-12}$	
$R_{\mathrm{epi,Co}}$ (s^{-1})	$(1.031 \pm 0.013) \times 10^{-11}$	
C_{Mn}	119.6 ± 1.9	123.9 ± 1.9
C_{Co}	32.98 ± 0.60	34.09 ± 0.62
r_σ	2.083 ± 0.037	2.085 ± 0.037
r_I	0.559 ± 0.017	0.559 ± 0.017
$\sigma_{0,\mathrm{Mn}}$ (b)	77.5 ± 1.4	77.5 ± 1.4
$I_{0,\mathrm{Mn}}(\alpha)$ (b)	43.1 ± 1.2	43.1 ± 1.2
$Q_{0,\mathrm{Mn}}(\alpha)$ (b)	0.557 ± 0.024	0.556 ± 0.023

at $v = 2200$ m/s, and the resonance integral $I_0(\alpha)$. A Maxwellian-energy distribution is assumed for the thermal neutrons and a $1/E^{1+\alpha}$ shape in the epithermal part of the spectrum. Activation by fission neutrons is neglected.

Experimentally, R can be assessed by activating the bare sample, R_{epi} by activation of the sample shielded by cadmium. Due to the shape of the (n,γ) cross section of cadmium, the transmission characteristics of a cadmium shield can be described in good approximation by a step function, whereby neutrons below the cadmium cut-off energy E_{Cd} (thermal neutrons) are considered as completely absorbed, while neutrons with energy above E_{Cd} (epithermal and fast neutrons) are fully transmitted. The exact value of E_{Cd} depends on the particular geometry and wall thickness of the cadmium case [38]. The value of $E_{\mathrm{Cd}} = 0.55$ eV is typically used and was adopted in our experiment. The thermal-activation rate is then calculated as the difference of the activation rates of the bare sample and the Cd-shielded sample:

$$R_{\mathrm{th}} = R - R_{\mathrm{epi}} = R - \frac{\hat{R}_{\mathrm{epi}}}{F_{\mathrm{Cd}}}. \tag{6}$$

It has to be noted that the experimentally measured epithermal-activation rate $\hat{R}_{\mathrm{epi}}$ of the cadmium-covered sample might be lower than in the uncovered case if there is a significant overlap between the resonances of cadmium and of the target isotope. This is corrected by the cadmium transmission factor F_{Cd}, defined as the ratio between the epithermal-activation rates with and without the cadmium shield. F_{Cd} differs from unity only for a small number of nuclides [38] and because no values of F_{Cd} were found in the literature for the relevant reactions ^{53}Mn(n,γ) and ^{59}Co(n,γ), during the data evaluation it was assumed to be $F_{\mathrm{Cd}} = 1$ and thus $R_{\mathrm{epi}} \approx \hat{R}_{\mathrm{epi}}$.

Combining Eqs. (5) and (6), the measured cross-section ratio r_σ can be expressed as [39]

$$r_\sigma = \frac{(R_{\mathrm{Mn}} - R_{\mathrm{epi,Mn}})}{(R_{\mathrm{Co}} - R_{\mathrm{epi,Co}})} \frac{g_{w,\mathrm{Co}}}{g_{w,\mathrm{Mn}}} \frac{G_{\mathrm{th,Co}}}{G_{\mathrm{th,Mn}}}. \tag{7}$$

The thermal-neutron self-shielding factors $G_{\mathrm{th,Mn}}$ and $G_{\mathrm{th,Co}}$ were assumed to be identical for reasons described in Sec. III A and thus, cancel out in Eq. (7). The Westcott factor $g_{w,\mathrm{Mn}}$ is not known and thus, was assumed to be unity in the evaluation. For $g_{w,\mathrm{Co}}$ the value of 1.004 [9] was adopted. The calculated values of r_σ and of the corresponding cross sections $\sigma_{0,\mathrm{Mn}}$ based on $\sigma_{0,\mathrm{Co}}$ are listed in Table VI.

Analogous to Eq. (7), the ratio of the resonance integrals r_I can be obtained using the following relationship [39]:

$$r_I = \frac{\left(C_{\mathrm{Co}} - F_{\mathrm{Cd,Co}}^{-1}\right) G_{\mathrm{epi,Co}}}{\left(C_{\mathrm{Mn}} - F_{\mathrm{Cd,Mn}}^{-1}\right) G_{\mathrm{epi,Mn}}} \frac{g_{w,\mathrm{Mn}}}{g_{w,\mathrm{Co}}} \frac{\sigma_{0,\mathrm{Mn}}}{\sigma_{0,\mathrm{Co}}} \frac{G_{\mathrm{th,Mn}}}{G_{\mathrm{th,Co}}}. \tag{8}$$

As discussed earlier, both the thermal- and epithermal-neutron self-shielding factors were assumed to cancel out in the equation and F_{Cd} was set to unity for both reactions. The resonance integral $I_0(\alpha)$ for the experimental neutron spectrum characterized by the epithermal-spectrum shape factor α can be calculated from the resonance integral I_0 for the ideal epithermal spectrum with $1/E$ shape using the effective resonance model [40]

$$I_0(\alpha) = \left(\frac{I_0 - 0.429 g_w \sigma_0}{(\bar{E}_r)^\alpha} + \frac{0.429 g_w \sigma_0}{(2\alpha + 1)(E_{\mathrm{Cd}})^\alpha} \right), \tag{9}$$

where $\bar{E}_r$ is the effective resonance energy as defined in [41]. The unit of $\bar{E}_r$ and E_{Cd} is eV. The literature value $\bar{E}_r = 136 \pm 7$ eV for ^{59}Co [42] was adopted. The evaluation of Eq. (9) yields a resonance integral of ^{59}Co of $I_{0,\mathrm{Co}}(\alpha) = 77.1 \pm 1.8$ b. The calculated values of r_I and as well as the resulting resonance integral $I_{0,\mathrm{Mn}}(\alpha)$ are given in Table VI. The ratio of the resonance integral and the thermal-neutron cross section $Q_{0,\mathrm{Co}}(\alpha)$ is additionally listed in Table VI.

IV. RESULTS AND DISCUSSION

Table VII presents the resulting ^{53}Mn capture cross sections σ_0 at $v = 2200$ m/s and the resonance integral $I_0(\alpha)$ as measured in our experiment and gives an overview of previous available literature data. Arithmetical average of the three cold-neutron activation values or the two reactor activation values obtained in each experiment (see Tables IV and VI) was built. The difference between these σ_0 values for the cold- and thermal-neutron activation is approximately 2.0 b (≈2.5%), which corresponds to around two standard deviations of the deduced values. We suggest a value of $\sigma_0 = 76.5 \pm 1.4$ b as the value of the thermal-neutron capture cross section of ^{53}Mn. The achieved accuracy of less than 2% is almost one order of magnitude better than in previous measurements and comparable with thermal-neutron cross-section uncertainties of stable nuclides.

The here selected approach, which is based on relative cross-section measurements against well-known reference cross sections, will generally minimize the magnitude of the involved uncertainty sources. We will discuss here in detail a

TABLE VII. Values of σ_0 and I_0 for the reaction ^{53}Mn(n,γ) measured in our activation experiments and previously reported values.

	σ_0 (b)	I_0 (b)
Cold-neutron activation (this work)	75.44 ± 0.94	—
Reactor activation (this work)	77.5 ± 1.0	43.1 ± 1.2 ($\alpha = 0.025$)
Average (this work)	76.5 ± 1.4	43.1 ± 1.2 ($\alpha = 0.025$)
Millard, Jr. (1965) [5]	170	—
(with $t_{1/2} = 3.7$ Ma)	95 ± 29	
Honda *et al.* (1971) [7]	82 ± 7	—
Wölfle *et al.* [8]	66 ± 7	<125
Mughabghab (6th ed.) [9]	70 ± 10	*30* $\pm$ *5*[a]

[a]See explanation in text.

possible additional contribution to the uncertainty budget. The determination of the total number of target atoms by ICP-MS cannot be the cause of the observed discrepancy, since the same samples prepared from one solution were used in both experiments. Furthermore, the evaluation generally does not use the absolute atomic numbers, but only the isotopic ratio of ^{53}Mn and ^{59}Co.

Even if Eq. (7) contains the terms $R-R_{\mathrm{epi}}$ and, thus, is formally dependent on the difference of the absolute number of atom in samples 1 (or 2) and 3, the influence of of $R_{\mathrm{epi}} \approx 0.01R$ to the uncertainty budget is negligible under the chosen experimental conditions. Neither γ-ray spectrometry can be responsible for the discrepancy in the view of the authors. All γ-ray measurements were performed with the same detector and sample holder, thus utilizing identical geometrical conditions for all measurements. The efficiency calibration itself was performed with a calibration source prepared in the same manner as the measured samples, thus accounting for true coincidence summing, volume effects, and self-attenuation in the best possible way.

Since the individual values of σ_0 within the particular activation experiment agree perfectly, we assume the discrepancy is caused by a systematic effect, which does not make the two activation measurements fully comparable at the current state of analysis. In our opinion, the result of the cold-neutron activation is more reliable due to the larger number of approximations and assumptions necessary for the proper evaluation of the reactor activation, e.g., about the Westcott factor or cadmium transmission factor of ^{53}Mn which are not known.

The reported values of σ_0 of ^{53}Mn agree reasonably with all previously reported measurements and their weighted average given in [9] as shown in Table VII. Our values stand almost exactly in the middle between the two newer measurements of Honda *et al.* [7] and Wölfle *et al.* [8] and are within 1 and 1.5 of their reported standard deviations, respectively. Millard [5] expressed the cross section of ^{53}Mn as a function of its half-life; the original value of 170 b reported in his paper was based on the ^{53}Mn half-life value of 2 Ma assumed at that time. The re-evaluation using the current adopted value of 3.7 Ma [43] yields 95 ± 29 b which is still higher, but compatible with our values within one standard deviation.

Regarding the resonance integral, no experimental values were found in the literature except for the upper limit stated by Wölfle *et al.* [8] with respect to the thermal-neutron capture cross section and the resonance integral of ^{64}Zn. The value of 30 ± 5 b listed in [9] is lower than our measured resonance integral, but it remains somewhat obscure as its original reference is not given in the corresponding literature list. It should be noted that our value of the resonance integral is strictly valid only for the irradiation conditions on the used sample position, characterized by the epithermal-spectrum shape factor $\alpha = 0.025$. The usually reported resonance integral I_0 for $\alpha = 0$ is expected to be smaller by less than 5%, but the corresponding transformation could not be performed due to the lack of data on the cross-section shape of ^{53}Mn.

The resonance integral can be used to improve the predictions of the cross-section shape in the resolved and unresolved resonance range, e.g., in future versions of the TENDL library, until a differential measurement of the capture cross section becomes available. With $Q_0(\alpha) \approx 0.6$, we expect rather weak resonances and the beginning of the resolved resonance range in the keV energy domain. This conclusion is supported by a recent measurement of the 30 keV Maxwellian-averaged capture cross section for the reaction ^{53}Mn(n,γ) which showed the MACS is low ($\approx$0.05%), compared to the thermal-neutron capture cross section [44].

ACKNOWLEDGMENTS

The authors would like to thank Dominik Herrmann for the designing and manufacturing of the sample holder for cold-neutron activation. Irradiation on the LVR-15 reactor was supported by the Ministry of Education, Youth and Sports of the Czech Republic under the Project No. LM2015074. The PSI authors did not receive any specific grant to perform the here presented research work.

[1] F.-K. Thielemann, K. Nomoto, and M.-A. Hashimoto, Astrophys. J. **460**, 408 (1996).
[2] S. Sahijpal, J. Astrophys. Astron. **35**, 121 (2014).
[3] D. P. Glavin, A. Kubny, E. Jagoutz, and G. W. Lugmair, Meteorit. Planet. Sci. **39**, 693 (2004).
[4] J. Schaefer, T. Faestermann, G. Herzog, K. Knie, G. Korschinek, J. Masarik, A. Meier, M. Poutivtsev, G. Rugel, and C. Schluchter, Earth Planet. Sci. Lett. **251**, 334 (2006).
[5] H. T. Millard, Jr., Science **147**, 503 (1965).
[6] M. Imamura, H. Matsuda, K. Horie, and M. Honda, Earth Planet. Sci. Lett. **6**, 165 (1969).
[7] M. Honda and M. Imamura, Phys. Rev. C **4**, 1182 (1971).
[8] R. Wölfle, Radiochim. Acta **18**, 207 (1972).

[9] S. F. Mughabghab, *Atlas of Neutron Resonances, Resonance Properties and Thermal Cross Sections Z = 1−60*, 6th ed. Vol. 1 (Elsevier, 2018).

[10] A. Koning and D. Rochman, Nucl. Data Sheets **113**, 2841 (2012).

[11] M. Fleming, J. Sublet, J. Kopecky, D. Rochman, and A. Koning, Probing experimental and systematic trends of the neutron-induced TENDL-2014 nuclear data library, Technical Report No. UKAEA-R(15)29 (CCFE, 2015).

[12] J.-Ch. Sublet, A. Koning, D. Rochman, M. Fleming, and M. Gilbert, TENDL-2015: Delivering Both Completeness and Robustness, in *Advances in Nuclear Nonproliferation Technology and Policy Conference, Santa Fe, New Mexico* (American Nuclear Society, 2016).

[13] D. Rochman, A. Koning, J. Sublet, M. Fleming, E. Bauge, S. Hilaire, P. Romain, B. Morillon, H. Duarte, S. Goriely, S. van der Marck, H. Sjöstrand, S. Pomp, N. Dzysiuk, O. Cabellos, H. Ferroukhi, and A. Vasiliev, EPJ Web Conf. **146**, 02006 (2017).

[14] A. Koning, D. Rochman, J.-C. Sublet, N. Dzysiuk, M. Fleming, and S. van der Marck, Nucl. Data Sheets **155**, 1 (2019).

[15] P. Englert, U. Herpers, R. Sarafin, and S. Vogt, J. Radioanal. Nucl. Chem. **113**, 119 (1987).

[16] V. E. Yants, S. G. Lebedev, and N. M. Sobolevsky, Cosmic Research **55**, 333 (2017).

[17] D. Schumann and J. Neuhausen, J. Phys. G **35**, 014046 (2007).

[18] D. Schumann, J. Neuhausen, J. Eikenberg, M. Rüthi, M. Wohlmuther, P. W. Kubik, H.-A. Synal, M. V. Alfimov, G. Korschinek, G. Rugel, and T. Faestermann, Radiochim. Acta **97**, 123 (2009).

[19] Evaluation of measurement data — Guide to the expression of Uncertainty in Measurement, Technical Report No. JCGM 100:2008 (Joint Committee for Guides in Metrology, 2008).

[20] M. Ayranov and D. Schumann, J. Radioanal. Nucl. Chem. **286**, 649 (2010).

[21] O. Reinitz, *Tagungsbericht 4. VDI Fachtagung Messunsicherheit praxisgerecht bestimmen, 12./13.11.2008*, Erfurt, 2008.

[22] A.-L. Hauswaldt, O. Rienitz, R. Jährling, N. Fischer, D. Schiel, G. Labarraque, and B. Magnusson, Accred. Qual. Assur. **17**, 129 (2011).

[23] J. Vogl and W. Pritzkow, MAPAN **25**, 135 (2010).

[24] W. R. Shields, T. J. Murphy, E. J. Catanzaro, and E. L. Garner, J. Res. Natl. Inst. Stan. **70A**, 193 (1966).

[25] J. Fonslet, S. Tietze, A. I. Jensen, S. A. Graves, and G. W. Severin, Appl. Radiat. Isot. **121**, 38 (2017).

[26] S. Weyer and J. Schwieters, Int. J. Mass Spectrom. **226**, 355 (2003).

[27] W. Russell, D. Papanastassiou, and T. Tombrello, Geochim. Cosmochim. Acta **42**, 1075 (1978).

[28] G. Audi, M. Wang, A. Wapstra, F. Kondev, M. MacCormick, X. Xu, and B. Pfeiffer, Chin. Phys. C **36**, 1287 (2012).

[29] P. Taylor, R. Maeck, and P. D. Bièvre, Int. J. Mass Spectrom. Ion Processes **121**, 111 (1992).

[30] A. Kaestner, S. Hartmann, G. Kuhne, G. Frei, C. Grünzweig, L. Josic, F. Schmid, and E. Lehmann, Nucl. Instrum. Methods Phys. Res. A **659**, 387 (2011).

[31] P. Vontobel (private communications) (2017).

[32] M. Koleška, Z. Lahodová, J. Šoltés, L. Viererbl, J. Ernest, M. Vinš, and J. Stehno, J. Radioanal. Nucl. Chem. **305**, 51 (2015).

[33] T. Goorley, M. James, T. Booth, F. Brown, J. Bull, L. J. Cox, J. Durkee, J. Elson, M. Fensin, R. A. Forster, J. Hendricks, H. G. Hughes, R. Johns, B. Kiedrowski, R. Martz, S. Mashnik, G. McKinney, D. Pelowitz, R. Prael, J. Sweezy, L. Waters, T. Wilcox, and T. Zukaitis, Nucl. Technol. **180**, 298 (2012).

[34] STAYSL PNNL Suite v1.2.0, developed by the Nuclear Data Section of the IAEA (2013).

[35] Decay Data Evaluation Project (DDEP)—tables of recommended data, available online.

[36] O. T. Hogdahl, Proceedings of the Symposium of Radiochemical Methods of Analysis, Salzburg (1964).

[37] S. Pomme, F. Hardeman, P. Robouch, N. Etxebarria, and G. Arana, Neutron activation analysis with K0-standardization: General formalism and procedure, Technical Report No. BLG-700 (SCK-KEN, 1997).

[38] A. Trkov and V. Radulović, J. Radioanal. Nucl. Chem. **304**, 763 (2015).

[39] M. Karadag and H. Yücel, Ann. Nucl. Energy **31**, 1285 (2004).

[40] F. D. Corte, L. Moens, S. Jovanović, A. Simonits, and A. D. Wispelaere, J. Radioanal. Nucl. Chem. **102**, 37 (1986).

[41] T. B. Ryves, Metrologia **5**, 119 (1969).

[42] S. Jovanović, F. D. Corte, A. Simonits, L. Moens, P. Vukotić, and J. Hoste, J. Radioanal. Nucl. Chem. **113**, 177 (1987).

[43] H. Junde, Nucl. Data Sheets **110**, 2689 (2009).

[44] J. Ulrich, M. Ayranov, O. Aviv, A. Barak, D. Berkovits, Y. Buzaglo, H. Dafna, B. Kaizer, N. Kivel, D. Kijel, A. Kreisel, M. Paul, E. Peretz, D. Rochman, D. Schumann, P. Sprung, M. Tessler, A. Türler, L. Weissman, Z. Yungrais, and R. Dressler, Phys. Rev. Lett. (to be published) (2020).